Int. J. Heat Mass Transfer. Vol. 33, No. 6, pp. 1233–1245, 1990
Printed in Great Britain

0017-9310/90 $3.00 + 0.00

Comparison of predicted and measured mixed convection heat transfer from an array of discrete sources in a horizontal rectangular channel

H. V. MAHANEY, F. P. INCROPERA and S. RAMADHYANI
Heat Transfer Laboratory, School of Mechanical Engineering, Purdue University, West Lafayette, IN 47907, U.S.A.

(*Received* 19 *April* 1989 *and in final form* 18 *September* 1989)

Abstract—Experiments and supporting three-dimensional computations have been performed to investigate mixed convection heat transfer from a four-row, in-line array of 12, square heat sources which are flush mounted to the lower wall of a horizontal, rectangular channel. The experimental data encompass heat transfer regimes characterized by pure natural convection, mixed convection, laminar forced convection, and the initiation of transition to turbulence. The variation of the row-average Nusselt number with Reynolds number exhibits a minimum, suggesting that, due to buoyancy-induced flow, heat transfer may be enhanced and pumping power requirements reduced by reducing the flow rate. Appropriate scaling parameters are introduced to characterize the strength of the buoyancy-induced secondary flow and to delineate conditions for which it is significant.

INTRODUCTION

A MAJOR driving force in the development of digital computers has been the achievement of ever larger scales of integration for monolithic circuits on a silicon chip. The attendant increase in heat dissipation within the chips, as well as the tendency to closely space chips in planar arrays, has placed stringent requirements on thermal management and has stimulated consideration of liquid cooling options. From the standpoint of heat transfer, the problem may be viewed as one involving convection from small, discrete sources mounted on a substrate that may be either a good or a poor thermal conductor.

An early study of forced convection heat transfer from a single, flush-mounted heat source was performed by Baker [1], who considered silicone oil and R-113 in parallel flow over rectangular sources with surface areas ranging from 1 to 200 mm^2. Convection coefficients increased significantly with decreasing area, and for the smallest sources data substantially exceeded predictions based on a two-dimensional boundary-layer model. The discrepancy was attributed to three-dimensional convection and substrate conduction effects, both of which become more pronounced with decreasing heater size. More recently, Samant and Simon [2] performed experiments for a 0.25 mm long by 2.0 mm wide heater mounted flush with one wall of a rectangular duct and, without boiling, achieved heat fluxes up to 200 W cm^{-2} for R-113 at large Reynolds numbers ($Re_D \approx 2 \times 10^5$).

The effects of combined convection and conduction from in-line heaters, flush mounted to one wall of a parallel-plate channel, have been considered numerically in Ramadhyani *et al.* [3] and Moffatt *et al.* [4] for laminar and turbulent flows, respectively. The two-dimensional, forced convection simulations presumed infinite heater length in the cross-stream direction and revealed conditions for which wall conduction was important and thermal boundary layer development on the upstream source had a significant influence on convection heat transfer from the downstream source. Predictions based on the two-dimensional, forced convection model with heat transfer data for a single 12.7 mm square heat source and for a 4×3 array of heat sources were compared in ref. [5]. The experiments were performed for water and FC-77, with the heater(s) embedded in the bottom wall of a horizontal channel. Excellent agreement obtained for turbulent flow suggested that three-dimensional convection effects were negligible, while significant underprediction of the data for laminar flow suggested that heat transfer was being enhanced by thermal instabilities and buoyancy-driven secondary flows.

The effect of buoyancy on convection heat transfer in laminar, horizontal channel flows is well known for continuously heated surfaces. Bottom heating induces a thermal instability which is manifested by ascending plumes of warm fluid and the development of longitudinal vortices. The onset of the thermal instability has been correlated [6], and the ensuing mixed convection flow has been predicted [7, 8]. In the mixed convection regime, Nusselt numbers are as much as six times larger than those corresponding to pure forced convection [9, 10], while friction factors are only slightly ($\lesssim 40\%$) larger [7].

The fact that mixed convection flows offer the potential for significant heat transfer enhancement

NOMENCLATURE

A_h	heater surface area, L_h^2
AR	aspect ratio, W/H
c_p	specific heat
D	duct hydraulic diameter
d_2, d_3	Rayleigh number exponents in natural convection correlations
g	gravitational acceleration
Gr	Grashof number, $g\beta\Delta TL_h^3/\nu^2$
Gr^*	modified Grashof number, $g\beta\bar{q}L_h^4/k\nu^2$
$\bar{h}_j$	average heat transfer coefficient for heater row j
H	duct height
k	fluid thermal conductivity
L_h	heater length
m	slope
$\overline{Nu}_j$	average Nusselt number for heater row j
$\bar{P}(z)$	mean pressure in duct cross section
$p(x,y,z)$	variation about mean pressure
Pe	Peclet number, $Re\ Pr$
Pr	Prandtl number, $c_p\mu/k$
$\bar{q}$	average heat flux, Q/A_h
Q	total power dissipation
Q_c	corrected power dissipation
Ra	Rayleigh number, $Gr\ Pr$
Ra^*	modified Rayleigh number, $Gr^*\ Pr$
Re	Reynolds number, $w_m L_h/\nu$
Re_D	Reynolds number, $w_m D/\nu$
S	spanwise and longitudinal spacing between neighboring edges of adjoining heaters
T	temperature
$T_{m,j}$	mixed mean fluid temperature just upstream of heater row j
u, v, w	spanwise, vertical, and longitudinal fluid velocities
w_m	mean longitudinal velocity
W	duct width
x, y, z	spanwise, vertical, and longitudinal duct coordinates.

Greek symbols

β	thermal expansion coefficient
μ	viscosity
ν	kinematic viscosity
ρ	fluid density.

Subscripts

Cu	copper
F	forced convection
h	heater
i	insulation
j	heater row index ($j = 1, 2, 3, 4$)
N	natural convection
o	inlet
ref	reference temperature for buoyancy force (arithmetic mean value at upstream cross section)
s	substrate.

with only a modest penalty in pressure loss suggests that such flow conditions may be well suited to applications involving discrete heating. However, studies of mixed convection from discrete sources are limited to the work of Kennedy and Zebib [11] and Tomimura and Fujii [12]. For small heater strips flush mounted to the walls of a horizontal channel, Kennedy and Zebib observed longitudinal vortices due to heating at the bottom surface. Tomimura and Fujii applied a laminar, two-dimensional (y–z) model to an array of strip heaters flush mounted to the bottom wall of a parallel plate channel. For vertical and near-vertical orientations, the streamwise component of the buoyancy force was predicted to significantly enhance Nusselt numbers. However, for horizontal and near-horizontal configurations, the two-dimensional model was unable to predict the significant enhancement associated with the three-dimensional buoyancy-driven flow.

The foregoing review suggests a need for detailed studies of mixed convection heat transfer from discrete heaters in a horizontal channel. The objective of this work has been to perform such a study for laminar flow over an in-line array of heaters flush mounted to the bottom wall of the channel. Flow conditions and heat transfer have been predicted from a three-dimensional simulation, and the heat transfer results have been compared with experimental data obtained for water.

EXPERIMENTAL METHODS

The in-line heat source array of this study consisted of four rows of 12.7 mm × 12.7 mm heaters, with three heaters per row. The heater size is typical of today's VLSI chips, and an in-line 4 × 3 arrangement of heaters is representative of existing two-dimensional multichip arrays. Each heat source (Fig. 1) consisted of a 6.6 mm thick copper block soldered on one surface to a thick film resistor (Mini-Systems). Temperatures at the opposite surface were measured by copper–constantan thermocouples (0.127 mm wire diameter) which were inserted through the thickness of the copper block and soft-soldered to the spanwise center of the surface. One thermocouple was installed at the center of each copper block surface. Two additional thermocouples were installed in each of the four copper blocks along the center heater column of the array

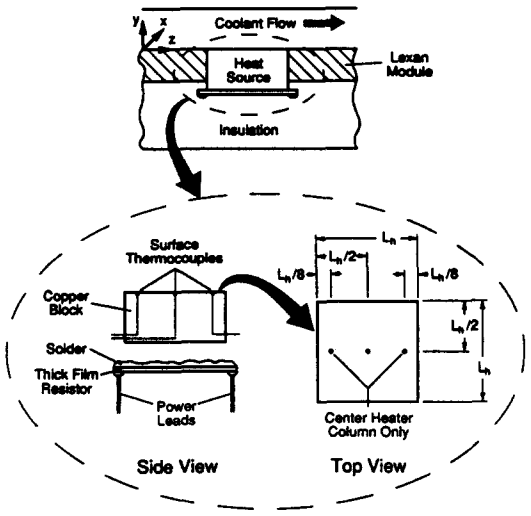

FIG. 1. Schematic of experimental heat source assembly.

at a distance of $L_h/8$ from the leading and trailing edges (Fig. 1). The heaters were flush mounted in a Lexan module ($k_s = 0.2$ W m^{-1} K^{-1}) having 12 broached holes, with in-line longitudinal and spanwise separations of $S = 3.18$ mm. A fine silica powder (Sylox 2) of low thermal conductivity ($k_i = 0.02$ W m^{-1} K^{-1}) was used to insulate the sources from the surroundings. The module was, in turn, flush mounted to the bottom wall of a flow channel (Fig. 2) of 50.5 mm width and 11.8 mm height ($D = 19.1$ mm, $AR = 4.3$). The module was located at a downstream distance of 611 mm from the flow straightener. Details of the flow loop and data acquisition procedures are described in ref. [5].

All of the experiments were conducted under conditions of equal heat dissipation (Q) in each of the heaters. Data were reduced in terms of an average Nusselt number for heater row j

$$\overline{Nu}_j = \frac{\bar{h}_j L_h}{k} = \frac{Q_c L_h}{A_h(\bar{T}_{h,j} - T_{m,j})k} \quad (1)$$

for which the heat source length and surface area are

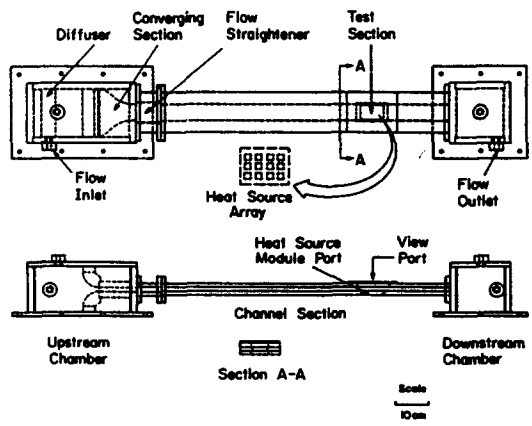

FIG. 2. Schematic of experimental flow channel.

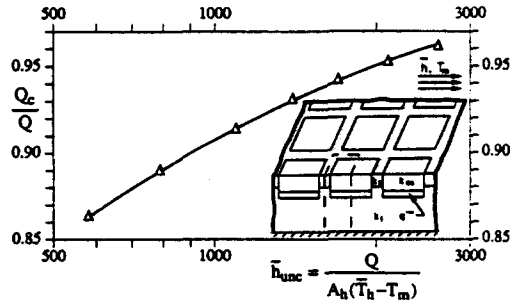

FIG. 3. Correction factor to account for three-dimensional conjugate heat transfer in the substrate. Inset: module geometry.

$L_h = 12.7$ mm and $A_h = 161$ mm^2. The corrected heat dissipation rate Q_c, which represents the heat transferred to the fluid directly through the heater face, accounts for substrate conduction losses. The power dissipation was corrected by utilizing a three-dimensional conduction analysis of the heater module (Fig. 3). By assuming a uniform heat transfer coefficient and a heater array which is infinite in the longitudinal and spanwise directions, the resultant symmetry allows the computational domain to be reduced to the region bordered by the dashed lines as shown in the inset of Fig. 3. The conduction analysis was used to estimate the ratio of convection heat transfer from the heater surface to the total power dissipation (Q_c/Q) as a function of the convection coefficient, and the results are represented in Fig. 3. This representation is particularly convenient for data reduction, since it allows an uncorrected heat transfer coefficient, $\bar{h}_{unc}$, which is based upon Q and is easily determined, to be corrected to that which is based on the actual heat transfer from the copper block to the fluid.

Since temperature variations between the three thermocouples in each center column heater were less than 0.5°C and area-weighted average surface temperatures were within 0.15°C of the center surface temperature, each heat source was essentially isothermal. The average convection coefficient for a given heater may therefore be based upon the single temperature measurement T_h for the center of the copper block and the mixed mean fluid temperature $T_{m,j}$ immediately upstream of the heater row. To indicate the row-by-row variation of heat transfer, the row-average Nusselt number of the three heaters in a row will be presented exclusively, where $\bar{T}_{h,j}$ is the average temperature of the three heaters in row j.

All thermophysical properties were evaluated at the fluid mixed mean temperature just upstream of the heater row, except for the viscosity, μ_h, which was evaluated at the row-average heater temperature and was used in the viscosity ratio, μ/μ_h, to account for non-constant property effects.

Experiments were performed for Reynolds numbers in the range $25 \leqslant Re \leqslant 2050$, for heater powers of 1, 2.5, 5 and 7.5 W, and for an inlet temperature

of $T_o \approx 15°C$. Corresponding values of the modified Rayleigh number ($Ra^* = g\beta\bar{q}L_h^4 Pr/kv^2$) ranged from 2.1×10^6 to 4.2×10^7. All experiments were performed in a horizontal channel with deionized and degassed water. An experimental uncertainty analysis using the technique of Kline and McClintock [13] revealed random uncertainties in Re and $\overline{Nu}_j$ to be less than 2% and from 2 to 6%, respectively, where the highest uncertainty in the Nusselt number is associated with the minimum power dissipation of $Q = 1$ W and large flow rates. Bias errors in the conjugate correction scheme are estimated to range from 2 to 5%, where the largest uncertainty is associated with the largest conjugate correction.

MATHEMATICAL MODEL AND NUMERICAL PROCEDURE

The buoyancy-driven flow is assumed to interact with a low Reynolds number (laminar) main flow to yield steady, three-dimensional, mixed convection conditions. Allowing the density in the body force term to vary linearly with temperature, while neglecting longitudinal diffusion and assuming all other properties to be constant, the governing equations may be expressed as

$$\frac{\partial u}{\partial x} + \frac{\partial v}{\partial y} + \frac{\partial w}{\partial z} = 0 \tag{2}$$

$$u\frac{\partial u}{\partial x} + v\frac{\partial u}{\partial y} + w\frac{\partial u}{\partial z} = -\frac{1}{\rho}\frac{\partial p}{\partial x} + \nu\left(\frac{\partial^2 u}{\partial x^2} + \frac{\partial^2 u}{\partial y^2}\right) \tag{3}$$

$$u\frac{\partial v}{\partial x} + v\frac{\partial v}{\partial y} + w\frac{\partial v}{\partial z} = -\frac{1}{\rho}\frac{\partial p}{\partial y} + \nu\left(\frac{\partial^2 v}{\partial x^2} + \frac{\partial^2 v}{\partial y^2}\right) + g\beta(T - T_{ref}) \tag{4}$$

$$u\frac{\partial w}{\partial x} + v\frac{\partial w}{\partial y} + w\frac{\partial w}{\partial z} = -\frac{1}{\rho}\frac{d\bar{P}}{dz} + \nu\left(\frac{\partial^2 w}{\partial x^2} + \frac{\partial^2 w}{\partial y^2}\right) \tag{5}$$

$$u\frac{\partial T}{\partial x} + v\frac{\partial T}{\partial y} + w\frac{\partial T}{\partial z} = \frac{k}{\rho c_p}\left(\frac{\partial^2 T}{\partial x^2} + \frac{\partial^2 T}{\partial y^2}\right). \tag{6}$$

A comparison of two-dimensional (y–z) elliptic and parabolic calculations indicates that longitudinal diffusion is negligible for the numerical computations of this study. In formulating the momentum equations, equations (3)–(5), the pressure has been represented as the sum of a cross-sectional mean pressure, $\bar{P}(z)$, which drives the main flow, and a perturbation about the mean, $p(x, y, z)$, which drives the cross-stream flow. In decoupling the longitudinal and cross-stream pressure gradients, it is tacitly assumed that $\partial\bar{P}/\partial z \gg \partial p/\partial z$.

Equations (2)–(6) were solved subject to (i) uniform fluid temperature and a fully developed, forced convection velocity profile at the duct entrance; (ii) no-slip and impermeable conditions at all channel walls; (iii) adiabatic conditions at all surfaces, except for locations occupied by discrete heat sources; and (iv) heat sources which are each isothermal in the spanwise direction and provide a spanwise average heat flux which is independent of longitudinal position. This thermal boundary condition simulates experimental conditions by providing equal power dissipation from each of the 12 heaters, while maintaining reasonably isothermal conditions for each heat source. For a given longitudinal position, the spanwise uniform heater temperatures vary with heater column due to the different convective conditions. By employing a spanwise symmetric heating pattern, the vertical plane through the duct center becomes a plane of symmetry and the computational domain is reduced to half of the duct cross section. At the plane of symmetry, the spanwise velocity component is zero, as are spanwise gradients of the temperature and the vertical and longitudinal velocity components.

Due to the multiplicity of length, velocity, and pressure scales, numerous options exist for non-dimensionalizing the foregoing equations and the corresponding boundary conditions. However, for a fixed geometry (S/L_h, H/L_h) and array size (3×4), each non-dimensionalization technique leads to the Reynolds, Prandtl and either the Grashof or Rayleigh numbers as pertinent dimensionless parameters. Hence, equations (2)–(6) were solved in dimensional form, while final results are presented in terms of the pertinent dimensionless parameters. Although the calculations were performed for a channel and heaters of specific dimensions, the results, when non-dimensionalized, are applicable to any geometrically similar system.

The solution scheme, which was specifically developed for the CDC Cyber 205, is an adaptation of the three-dimensional parabolic calculation procedure of Patankar and Spalding [14]. The governing partial differential equations are reduced to systems of simultaneous algebraic equations by a control-volume-based, finite-difference procedure [15] and linearized by evaluating the finite-difference coefficients from known upstream values. The sequence in which each of the governing equations is solved during a forward step in the marching integration is described in ref. [8]. The systems of algebraic finite-difference equations were solved using a vectorized Jacobi iterative technique. Since the coefficient structure of the pressure equations is not strongly diagonal-dominant, convergence rates were improved by using a checkerboard Jacobi scheme [16] and an additive correction technique along nodal rows and columns [17].

For each value of Ra^*, a parametric study of the influence of Reynolds number was conducted. For each of these parametric variations, the influence of grid fineness was tested at the lowest Reynolds number, which corresponds to the strongest sec-

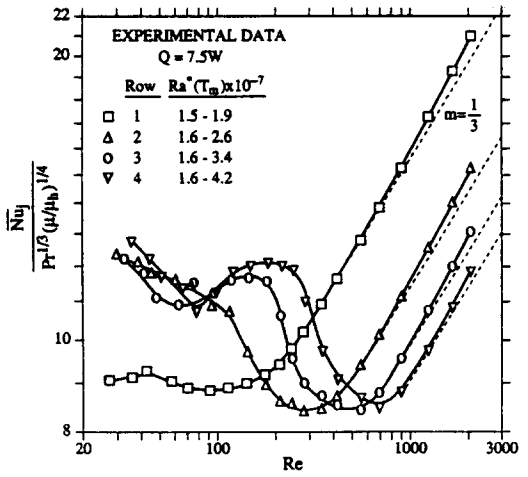

FIG. 4. Experimental results for the effect of Reynolds number on the row-average Nusselt number for $Q = 7.5$ W.

ondary flow and hence would require the finest grid. The grid study indicated that for $Ra^* \leqslant 3.0 \times 10^7$, average Nusselt numbers for the 12 heaters were within 3% for 40×123 and 60×165 cross-stream grids. The numbers refer, respectively, to the number of grid lines in the y- and x-directions. Thus, the 40×123 grid was used for the remainder of the calculations. However, for $Ra^* = 8.5 \times 10^7$ the finer grid was required for $Re \leqslant 800$. Each simulation for the 40×123 and the 60×165 grids typically required 1000 and 3600 CPU s, respectively, on the Cyber 205.

A non-uniform grid was employed in all three coordinate directions. In the x-direction, grid planes were clustered near points of discontinuity in the thermal boundary condition, while in the y-direction, grid planes were deployed symmetrically about the horizontal midplane of the channel with minimum grid spacing near the walls. Three hundred longitudinal steps were employed to march through the domain. Sixty steps were used to cover each heater, and 15 steps were used for each non-heated zone beyond the heater. Finer axial step sizes were employed near the leading edge of both of these regions.

Computations were performed for a geometry similar to that employed experimentally, except that the flow channel was assumed to be 50.8 mm wide and 12.7 mm high ($D = 20.3$ mm, $AR = 4$). Numerical parameter ranges include $125 \leqslant Re \leqslant 2500$, $4.7 \leqslant Pr \leqslant 8.3$ and $1.1 \times 10^7 \leqslant Ra^* \leqslant 8.5 \times 10^7$.

RESULTS

Experimental data obtained for a power dissipation of 7.5 W per heater are plotted in Fig. 4. The results for large values of Re are characteristic of pure forced convection. The functional dependence of the forced convection Nusselt number may be derived from the integral form of the boundary-layer energy equation. For flow between parallel plates, with a fully developed laminar velocity profile and a cubic temperature profile, it may be shown that

$$\overline{Nu}_F = C_1 \, Pe^{1/3}. \tag{7}$$

Experimental forced convection results for all four rows fall along this theoretical slope. Data for the largest Reynolds numbers lie just above this limit, indicating initiation of transition to turbulence. The reduction of heat transfer with row number in the forced convection regime results from thermal boundary-layer development due to upstream heating.

As the Reynolds number is decreased, heat transfer enhancement above the forced convection limit initially occurs for the fourth heater row. This behavior results from the onset of thermal instabilities and the development of secondary flow due to heating at the three upstream rows. However, the Nusselt number continues to decay with decreasing Reynolds number until a minimum is reached, where the reduction in $\overline{Nu}_4$ due to forced convection effects is balanced by an increase due to the buoyancy-driven secondary flow. With a further reduction of Reynolds number, the strength of the buoyancy-induced secondary flow increases and the corresponding enhancement more than offsets the decrease due to a reduction in the forced flow. Having achieved conditions dominated by mixed convection, a further decrease in Reynolds number results in decay of the forced convection component, transition to pure natural convection and a decreasing Nusselt number. The subsequent increase in $\overline{Nu}_4$ with decreasing Reynolds number for $Re \leqslant 75$ is attributed to substantial increases in the bulk temperature and variations of fluid properties. Although the data appear to be strongly Reynolds number dependent, the results will be shown to correspond to pure natural convection and the increase in Nusselt number to be due to substantial increases in the Rayleigh number. The wide Rayleigh number variation due to changes in fluid temperature is indicated in Fig. 4 for each heater row.

The transitions from pure forced convection to mixed convection to pure natural convection occur in a similar manner for the upstream rows. Since transition from forced to mixed convection results from the onset of thermal instabilities and from the cumulative development of secondary flows due to heating at all upstream rows, this transition occurs for each successive upstream row at a smaller Reynolds number. Due to the absence of heat transfer upstream of the first row, transition from forced to mixed convection for the first row results solely from the onset of thermal instabilities which occur at the first row. Thus, for the given Rayleigh number, significant enhancement above the minimum heat transfer rate does not occur with decreasing Reynolds number for the first row. However, with decreasing Reynolds number, substantial enhancement above the forced convection limits occurs for every row, including the first. The fact that the variation of the row average Nusselt number with Reynolds number exhibits a

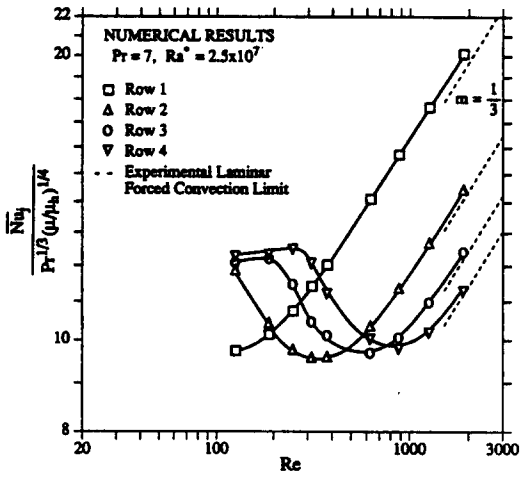

FIG. 5. Numerical prediction of the effect of Reynolds number on the row-average Nusselt number for $Ra^* = 2.5 \times 10^7$ and $Pr = 7$.

minimum for each row, suggests that heat transfer may be enhanced due to buoyancy-induced flow by reducing the flow rate and hence the pumping power requirements. The data associated with the smallest value of Re correspond to a flow rate of only $5.2\,l\,h^{-1}$.

Numerical results for $Ra^* = 2.5 \times 10^7$ and $Pr = 7$ are shown in Fig. 5, along with the experimental, laminar forced convection limits of Fig. 4. The viscosity ratio, $(\mu/\mu_h)^{1/4}$, is equal to unity for the constant property numerical predictions. The numerical predictions exhibit the appropriate forced convection, Reynolds number dependence and, compared to the experimental results, overpredict forced convection heat transfer for rows 1–4 by 4, 2, 1 and 0.5%, respectively. These percent differences are within the uncertainty in the experimental data.

As the Reynolds number is decreased, numerical results predict, in accord with the experimental data, heat transfer enhancement due to development of a buoyancy induced secondary flow, which initially occurs for the final heater row and progresses towards the first row. As seen in Figs. 4 and 5, enhancement at the fourth row occurs with a decreasing Reynolds number and provides for an increasing heat transfer rate which, before a maximum is achieved, exceeds that of the three upstream rows. Similarly, enhancement at the third and second rows occurs for successively smaller Reynolds numbers than that for the fourth row and yields heat transfer which exceeds that for all upstream rows. Figures 4 and 5 also indicate that for a decreasing Reynolds number, similar heat transfer rates are achieved for rows 2–4. Experimental and numerical results indicate heat transfer enhancement for row 1 such that, as the Reynolds number decreases, the Nusselt number asymptotes to a relatively constant value. Qualitative comparisons of Figs. 4 and 5, which include the relative positioning of the data for each row, cross-over points and slopes, and the magnitudes of enhancements, are good. Discrepancies between the experimental and numerical mixed convection results of Figs. 4 and 5 are attributed to the wide experimental variation of fluid properties, which corresponds to a row-by-row Rayleigh number variation which cannot be treated by the constant property, fixed Rayleigh number solution. Although variable properties could be incorporated into the numerical algorithm, this option was rejected due to the resultant increase in computation time, which would be in addition to the presently CPU-intensive constant property calculations. Numerical computations were not performed for Reynolds numbers as small as those achieved experimentally due to the corresponding grid refinement requirements and breakdown of the assumption of negligible longitudinal diffusion at very low Reynolds numbers.

For fully developed, forced convection flows the cross-stream velocities are zero and the row-average Nusselt number monotonically decreases with heater row. However, buoyancy forces induce cross-stream velocities that are extremely effective in advecting cold and warm fluid, respectively, to and from the surface and, as revealed by Figs. 4 and 5, in enhancing heat transfer. Cross-stream velocities and isotherms corresponding to the $Re = 312.5$ data point of Fig. 5 are given in Fig. 6. Cross-stream velocity vectors are shown at every alternate node, and the temperature difference between isotherms is 5°C. At the trailing edge of the first heater row (Fig. 6(a), $z/L_h = 1$) cooler, more dense fluid descends along the vertical wall ($x/L_h = 0$) and in the region between heaters ($1.25 \leqslant x/L_h \leqslant 1.5$), yielding locally enhanced heat transfer. This motion is accompanied by the ascension of adjacent warmer fluid, which is cooled and ultimately feeds the descending fluid. Although the unstable condition of warmer, less dense fluid beneath cooler, more dense fluid occurs across the entire bottom plate, a pronounced spanwise temperature gradient exists only at the heater edges. This gradient provides a region where the buoyancy force varies with x, as well as with y, thereby providing a source of vorticity. Thus, secondary flows initially develop at spanwise locations where discontinuities in the thermal boundary condition exist.

At the trailing edge of the non-heated region beyond the first heater row (Fig. 6(b), $z/L_h = 1.25$), the bottom plate temperature has substantially decreased. However, as shown by the velocity scale, which corresponds to the maximum cross-stream velocity at the given longitudinal position, the cross-stream velocities have increased with longitudinal position, even though the heating has been interrupted.

At the trailing edge of the second heater row (Fig. 6(c), $z/L_h = 2.25$), the three zones of ascending fluid have bifurcated and are feeding the two original downflows, as in Figs. 6(a) and (b), as well as three new zones of downward moving fluid ($x/L_h \approx 0.5, 1.0, 1.75$). These new downflows act to locally compress isotherms near the heated surface and to enhance heat

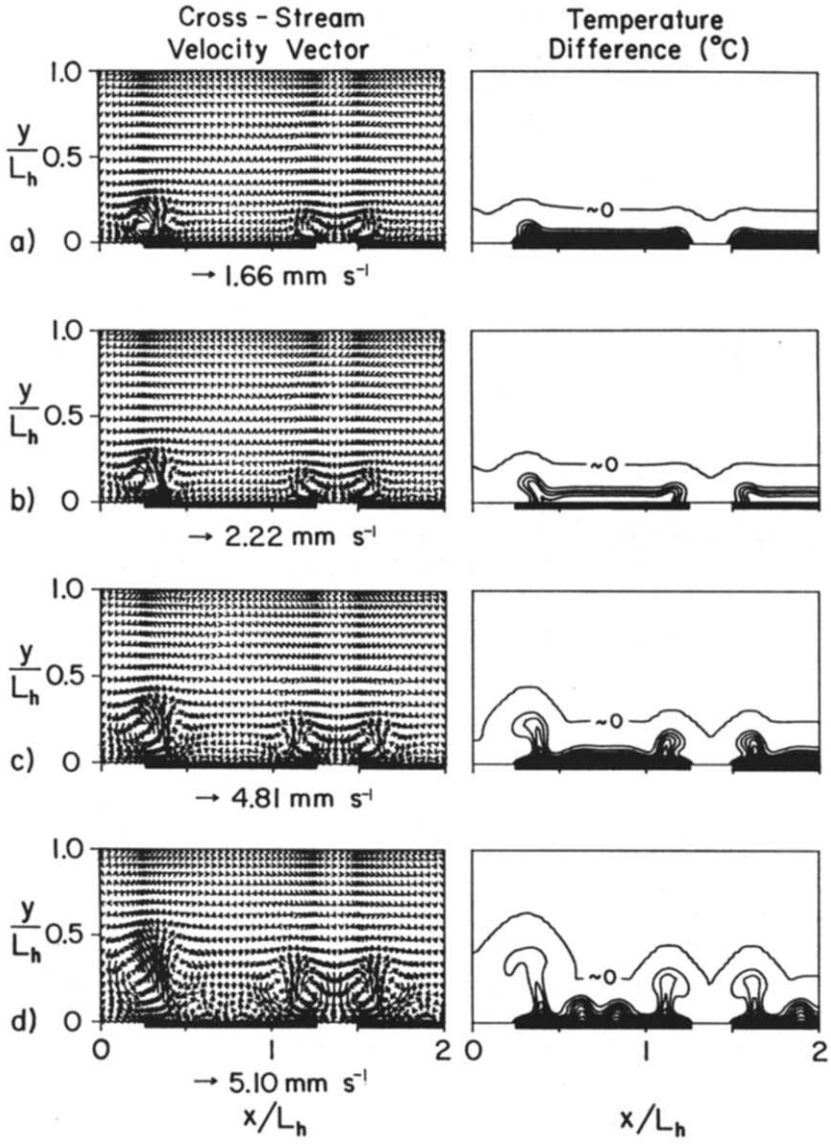

FIG. 6. Cross-stream velocity vectors and isotherms $(T-T_o)$ for $Ra^* = 2.5 \times 10^7$, $Re = 312.5$ and $Pr = 7$: (a) $z/L_h = 1.0$; (b) $z/L_h = 1.25$; (c) $z/L_h = 2.25$; (d) $z/L_h = 3.5$.

transfer. At the trailing edge of the third row (Fig. 6(d), $z/L_h = 3.5$), the three zones of ascending fluid have created two additional regions of downflow at $x/L_h \approx 0.75$ and 2.0, which also act to locally compress the isotherm lines and to enhance heat transfer. Conditions seen by the fourth heater row are similar to those of the third row (Fig. 6(d)).

Experimental data indicating the influence of varying the power dissipation per heater from 1 to 7.5 W are shown for rows 1–4 in Figs. 7(a)–(d), respectively. The experimental forced convection limits of rows 2–4 are also shown in Fig. 7(a) to facilitate comparisons between figures. Data agree with the theoretical slope for laminar forced convection, while data for the largest values of Re suggest the initiation of transition to turbulence. Due to temperature dependent fluid properties, the legend of Fig. 7 indicates that with increasing power dissipation, the Rayleigh number range associated with a prescribed power increases. Increasing the power dissipation enhances heat transfer and extends the Reynolds number range associated with mixed convection.

Numerical results indicating the influence of varying the Rayleigh number are shown for rows 1–4 in Figs. 8(a)–(d), respectively. The numerical forced convection limits of rows 2–4 are also shown in Fig. 8(a) to facilitate comparisons between figures. In accord with the experimental data, increasing the Rayleigh number enhances heat transfer and extends the Reynolds number range associated with mixed convection. Direct comparison of experimental and numerical results is complicated by the large Rayleigh

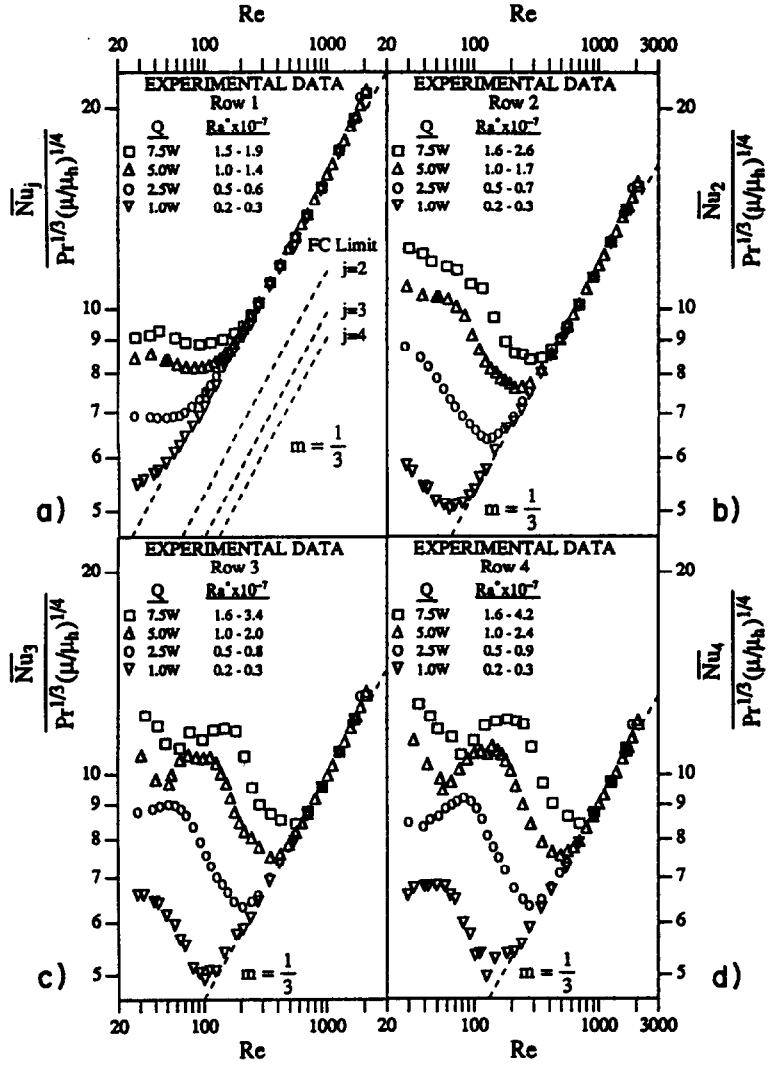

FIG. 7. Experimental results for the effect of Reynolds number and power dissipation on the row-average Nusselt number for (a) all rows, (b) row 2, (c) row 3, and (d) row 4.

number variation associated with the experimental data for a given power dissipation.

The similarity in the $\overline{Nu}$ vs Re distributions for varying values of Q, as shown in Fig. 7, suggests that data for different power dissipations may be collapsed by an appropriate choice of scaling parameters. The functional dependence of the mixed convection Nusselt number may be modelled as a superposition of Nusselt numbers for pure forced convection, $\overline{Nu}_F$, and pure natural convection, $\overline{Nu}_N$ [18], as

$$(\overline{Nu})^n = (\overline{Nu}_F)^n \pm (\overline{Nu}_N)^n. \tag{8}$$

The forced convection correlation is given by equation (7), while the appropriate natural convection correlation for a horizontal flat plate with a heated upper surface is

$$\overline{Nu}_N = C_2\, Ra^{d_2} = C_3\, Ra^{*d_3} \tag{9}$$

where $1/4 \leqslant d_2 \leqslant 1/3$ and $1/5 \leqslant d_3 \leqslant 1/4$. Many investigators present two correlating equations based on each of the limiting values of the exponents, with one correlation applied for Rayleigh numbers exceeding a specified value and the other correlation applied for Rayleigh numbers below the specified value [19]. However, Fishenden and Saunders [20] suggest that the exponent gradually increases as the Rayleigh number increases, while Chu and Goldstein [21] identify eight discrete heat flux transitions within a given Rayleigh number range. For the data of this study, the best correlation was achieved with an intermediate value of $d_3 = 2/9$. Substitution of equations (7) and (9) into equation (8) and rearrangement yields

$$\left(\frac{\overline{Nu}}{Pe^{1/3}}\right)^n = C_1^n \pm \left(\frac{C_3\, Ra^{*2/9}}{Pe^{1/3}}\right)^n. \tag{10}$$

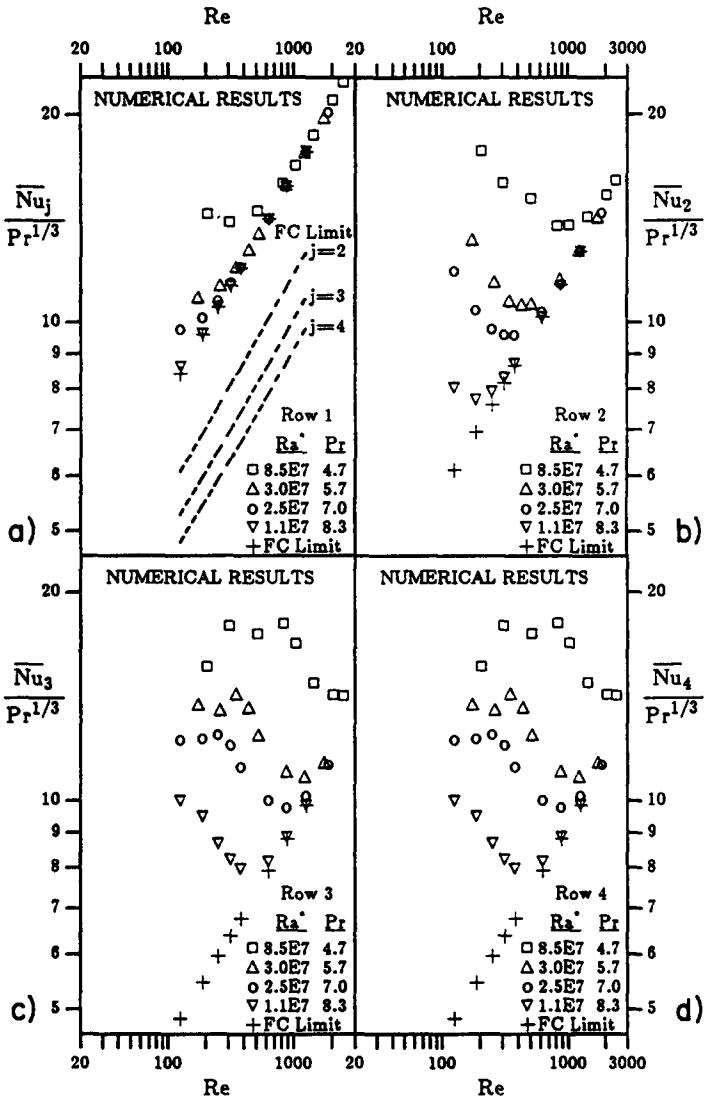

FIG. 8. Numerical prediction of the effect of Reynolds and Rayleigh numbers on the row-average Nusselt number for (a) all rows, (b) row 2, (c) row 3, and (d) row 4.

Thus, the ratio $\overline{Nu}/Pe^{1/3}$ is solely a function of $Ra^{*2/9}/Pe^{1/3}$ or, alternatively, by raising this mixed convection parameter to the $-9/2$ power, $\overline{Nu}/Pe^{1/3}$ is solely a function of $Pe^{3/2}/Ra^*$.

The experimental data of Fig. 7 are replotted in Fig. 9 using the derived scaling parameters. Data for power dissipations of 1–7.5 W collapse reasonably well when plotted in this manner. For small values of $Pe^{3/2}/Ra^*$, the results are asymptotic to a slope of $m = -2/9$, which is consistent with the natural convection correlation (equation (9)) and for which the Nusselt number is independent of Peclet number. For large values of $Pe^{3/2}/Ra^*$, the results collapse to horizontal lines which correspond to pure forced convection. The ordinate values of the horizontal asymptotes correspond to the constant C_1 of equation (7) if a viscosity ratio is included, and for rows 1–4, $C_1 \approx 1.56$, 1.14, 0.99 and 0.91, respectively. The reduction of C_1 with row number results from the thermal boundary layer which develops due to upstream heating. The diminishing change of C_1 with row number indicates that fully developed, forced convection conditions are being approached, but have not been reached by the fourth row. The slight deviation of the $Q = 1$ W data from data corresponding to $Q \geq 2.5$ W is attributed to the large uncertainties in measuring $(T_h - T_m)$ for small Q. Transition to turbulence occurs for large values of $Pe^{3/2}/Ra^*$. As seen in Fig. 7, transition to turbulence is primarily dependent upon the Reynolds number and a Rayleigh number dependence is not evident. Thus, transition for increasing values of $Q(Ra^*)$ occurs for decreasing values of $Pe^{3/2}/Ra^*$.

Regimes of significant mixed convection enhancement can be delineated. The onset of enhancement due to mixed convection, which is assumed to occur when the parameter $\overline{Nu_j}/Pe^{1/3}(\mu/\mu_h)^{0.25}$ exceeds the

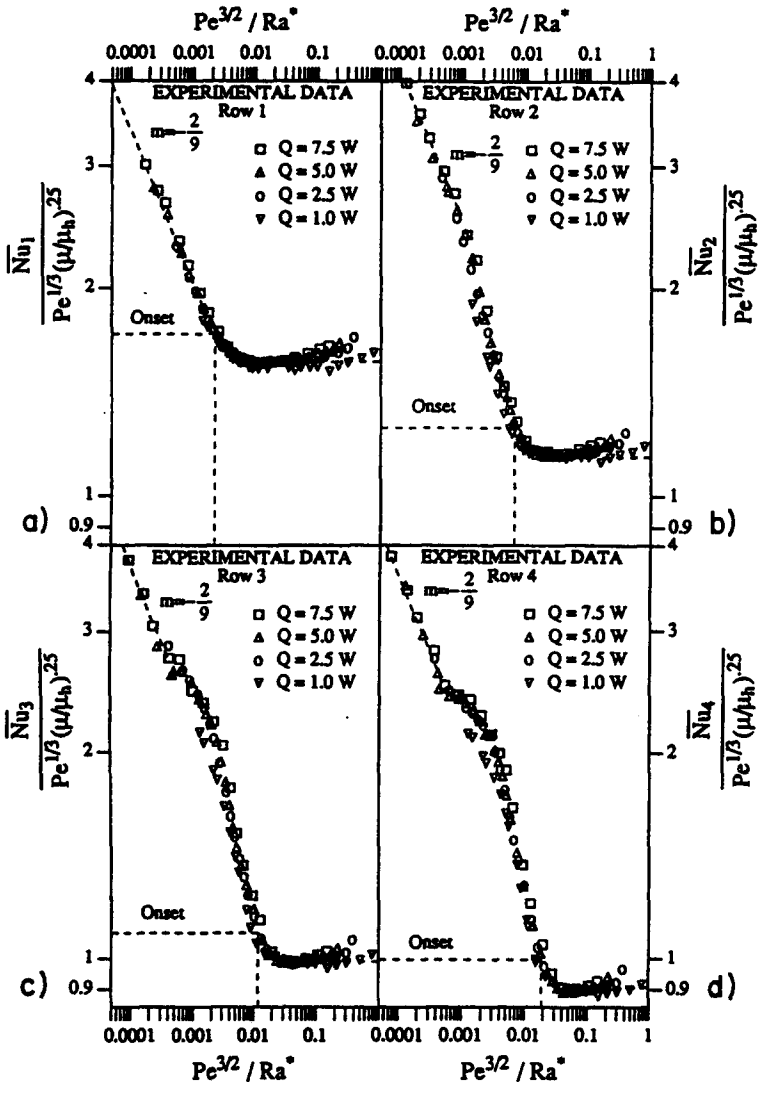

FIG. 9. Experimental row-average Nusselt numbers for $25 < Re < 2050$ and $1\ \text{W} \leqslant Q \leqslant 7.5\ \text{W}$ for (a) row 1, (b) row 2, (c) row 3, and (d) row 4.

forced convection limit of row j by 10%, corresponds to parameter values of $Pe^{3/2}/Ra^* = 0.0022$, 0.0065, 0.012 and 0.019 for rows 1–4, respectively. Figure 9 reveals increasing heat transfer enhancement above the forced convection limit with decreasing $Pe^{3/2}/Ra^*$. For the smallest mixed convection parameter values of this study, enhancement above the forced convection limit exceeds 300%.

The numerical results of Fig. 8 are replotted in Fig. 10 using the derived scaling parameters. Heretofore, numerical and experimental results have not been directly compared because the numerical results correspond to a fixed Rayleigh number, while due to non-constant property effects, the experimental data correspond to a wide, row-by-row Rayleigh number variation. However, by incorporating the Rayleigh number into the scaling parameters, direct comparison between numerical and experimental results is possible. Therefore, best-fit lines to the experimental data of Fig. 9 are also shown in Fig. 10, thus summarizing all of the numerical and experimental results in one figure. As before, the viscosity ratio is equal to unity for the constant property numerical predictions. The numerical results predict both the forced and natural convection limits and show excellent agreement with the experimental data.

Although the parametric influences of Re and Ra^* have been considered herein, the influence of Pr, S/L_h, H/L_h and the number of heater rows and columns has not been considered. Fluids currently under consideration for immersion cooling of electronic components have higher Prandtl numbers and higher coefficients of thermal expansion resulting in substantially higher Rayleigh numbers. The geometric parameters, S/L_h and H/L_h, are also expected to be important. The influence of S/L_h on two-dimensional

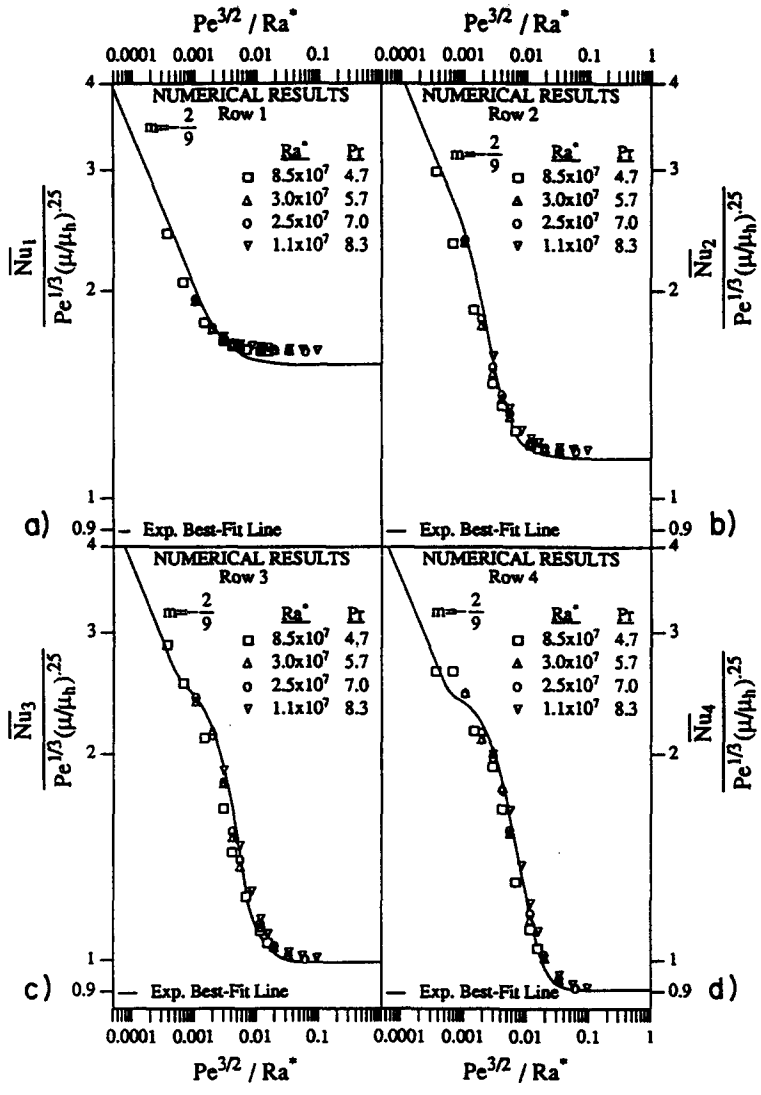

FIG. 10. Comparison of numerical and experimental row-average Nusselt numbers for (a) row 1, (b) row 2, (c) row 3, and (d) row 4.

(y–z) conjugate heat transfer from discrete heat sources flush mounted to the wall of a channel with laminar forced convection flow has been numerically demonstrated [3]. Since the column-by-column variation of flow and heat transfer characteristics was found to be small, the influence of the number of heater columns can be neglected. Since upstream propagation of influences is minimal for the conditions of this study, the results presented herein are directly applicable to arrays of four rows or less, and the results would also apply to the first four rows of a larger array.

CONCLUSIONS

A combined experimental and numerical study of mixed convection flow of water in a horizontal rectangular duct with a 3×4 array of discrete heat sources flush mounted to the lower wall has been performed. The variation of the row-average Nusselt number with Reynolds number exhibits a minimum, suggesting that, due to buoyancy-induced flow, heat transfer may be enhanced and pumping power requirements reduced by reducing the flow rate. Increasing the Rayleigh number enhances heat transfer above the forced convection limit and increases the Reynolds number range for which enhancement occurs.

Experimental and numerical results for a wide range of conditions collapse to a single curve for each heater row when $\overline{Nu}_j/Pe^{1/3}(\mu/\mu_h)^{0.25}$ is plotted against the mixed convection parameter $Pe^{3/2}/Ra^*$. The experimental data encompasses heat transfer regimes characterized by pure natural convection, mixed convection, laminar forced convection and the initiation of transition to turbulence. Mixed convection

effects are significant for heater rows 1–4 for $Pe^{3/2}/Ra^* \leqslant 0.0022$, 0.0065, 0.012 and 0.019, respectively, and for the conditions of this study provide up to 300% enhancement above the forced convection limit.

Acknowledgements—This work has been supported by the National Science Foundation under Grant No. CBT-8611840A1. One of us (H.V.M.) is grateful for support provided by a National Science Foundation Fellowship.

REFERENCES

1. E. Baker, Liquid cooling of microelectronic devices by free and forced convection, *Microelectron. Reliability* **11**, 213–222 (1972).
2. K. R. Samant and T. W. Simon, Heat transfer from a small, high-heat-flux patch to a subcooled turbulent flow, ASME Paper 86-HT-22 (1986).
3. S. Ramadhyani, D. F. Moffatt and F. P. Incropera, Conjugate heat transfer from small isothermal heat sources embedded in a large substrate, *Int. J. Heat Mass Transfer* **28**, 1945–1952 (1985).
4. D. F. Moffatt, S. Ramadhyani and F. P. Incropera, Conjugate heat transfer from wall embedded sources in turbulent channel flow. In *Heat Transfer in Electronic Equipment—1986*, ASME HTD-Vol. 57, pp. 177–182 (1986).
5. F. P. Incropera, J. S. Kerby, D. F. Moffatt and S. Ramadhyani, Convection heat transfer from discrete sources in a rectangular channel, *Int. J. Heat Mass Transfer* **29**, 1051–1058 (1986).
6. F. P. Incropera, A. L. Knox and J. A. Schutt, Onset of thermally driven secondary flow in horizontal rectangular ducts, *Proc. 8th Int. Heat Transfer Conf.*, Vol. 3, pp. 1395–1400. Hemisphere, Washington, DC (1986).
7. F. P. Incropera and J. A. Schutt, Numerical simulation of laminar mixed convection in the entrance region of horizontal rectangular ducts, *Numer. Heat Transfer* **8**, 707–729 (1985).
8. H. V. Mahaney, F. P. Incropera and S. Ramadhyani, Development of laminar mixed convection flow in a horizontal rectangular duct with uniform bottom heating, *Numer. Heat Transfer* **12**, 137–155 (1987).
9. D. G. Osborne and F. P. Incropera, Laminar, mixed convection heat transfer for flow between horizontal parallel plates with asymmetric heating, *Int. J. Heat Mass Transfer* **28**, 207–217 (1985).
10. F. P. Incropera, A. L. Knox and J. R. Maughan, Mixed-convection flow and heat transfer in the entry region of a horizontal rectangular duct, *J. Heat Transfer* **109**, 434–439 (1987).
11. K. J. Kennedy and A. Zebib, Combined free and forced convection between horizontal parallel planes: some case studies, *Int. J. Heat Mass Transfer* **26**, 471–474 (1983).
12. T. Tomimura and M. Fujii, Laminar mixed convection heat transfer between parallel plates with localized heat sources. In *Cooling Technology for Electronic Equipment* (Edited by W. Aung), pp. 233–247. Hemisphere, Washington, DC (1988).
13. S. J. Kline and F. A. McClintock, Describing uncertainties in single-sample experiments, *Mech. Engng* **75**, 3–8 (1953).
14. S. V. Patankar and D. B. Spalding, A calculational procedure for heat, mass and momentum transfer in three-dimensional parabolic flows, *Int. J. Heat Mass Transfer* **15**, 1787–1806 (1972).
15. S. V. Patankar, *Numerical Heat Transfer and Fluid Flow*. Hemisphere, Washington, DC (1980).
16. H. V. Mahaney, F. P. Incropera and S. Ramadhyani, Effect of wall heat flux distribution on laminar mixed convection in the entrance region of a horizontal rectangular duct, *Numer. Heat Transfer* **13**, 427–450 (1988).
17. B. R. Hutchinson and G. D. Raithby, A multigrid method based on the additive correction strategy, *Numer. Heat Transfer* **9**, 511–537 (1986).
18. S. W. Churchill and R. Usagi, A general expression for the correlation of rates of transfer and other phenomena, *A.I.Ch.E. Jl* **18**, 1121–1128 (1972).
19. F. P. Incropera and D. P. DeWitt, *Fundamentals of Heat and Mass Transfer* (2nd Edn), p. 433. Wiley, New York (1985).
20. M. Fishenden and O. A. Saunders, *An Introduction to Heat Transfer*, p. 96. Oxford University Press, Oxford (1950).
21. T. Y. Chu and R. J. Goldstein, Turbulent convection in a horizontal layer of water, *J. Fluid Mech.* **60**, 141–159 (1973).

COMPARAISON ENTRE CALCULS ET MESURES DE LA CONVECTION THERMIQUE MIXTE POUR UN ARRANGEMENT DE SOURCES DISCRETES DANS UN CANAL RECTANGULAIRE HORIZONTAL

Résumé—Des expériences et des calculs numériques tridimensionnels sont menés sur la convection thermique mixte pour quatre rangées en ligne de 12 sources thermiques carrées qui sont montées sur la paroi inférieure d'un canal rectangulaire horizontal. Les données expérimentales couvrent les régimes thermiques caractérisés par la convection naturelle pure, la convection mixte, la convection forcée laminaire et le début de la transition à la turbulence. La variation du nombre de Nusselt moyen par rangée en fonction du nombre de Reynolds montre un minimum, ce qui suggère qu'à cause de l'écoulement induit par le flottement, le transfert thermique peut être augmenté et la perte de charge être réduite par la diminution du débit de fluide. On introduit des paramètres appropriés de réduction pour caractériser l'importance de l'écoulement secondaire de flottement et pour définir les conditions dans lesquelles il intervient activement.

VERGLEICH ZWISCHEN BERECHNETEM UND GEMESSENEM WÄRMEÜBERGANG BEI GEMISCHTER FREIER UND ERZWUNGENER KONVEKTION IN EINEM FELD VON EINZELNEN WÄRMEQUELLEN IN EINEM HORIZONTALEN, RECHTECKIGEN KANAL

Zusammenfassung—Es wurden Experimente und dreidimensionale numerische Berechnungen zur Untersuchung des Wärmeübergangs bei gemischter Konvektion durchgeführt. Ein 4-zeiliges Feld aus 12 quadratischen, fluchtend angeordneten Wärmequellen wird betrachtet, welche bündig mit der unteren Wand eines horizontalen rechteckigen Kanals abschließen. Die experimentellen Daten umfassen Bereiche des Wärmeübergangs, die charakteristisch sind für reine natürliche, gemischte, erzwungene laminare Konvektion und für den Beginn des Übergangs zur turbulenten Konvektion. Die Änderung der über die Zeile gemittelten Nusselt-Zahl mit der Reynolds-Zahl weist ein Minimum auf; dies legt nahe, daß sich der Wärmeübergang, bedingt durch die Auftriebsströmung, günstiger darstellt und die Pumpenleistung durch Verringerung des Durchflusses verringert werden kann. Entsprechende Skalierungsparameter werden eingeführt, um die Stärke der durch Auftriebskräfte induzierten Sekundärströmung zu beschreiben und die Voraussetzungen abzugrenzen, für welche sie bedeutsam ist.

СОПОСТАВЛЕНИЕ РАССЧИТАННОГО И ИЗМЕРЕННОГО СМЕШАННОКОНВЕКТИВНОГО ТЕПЛОПЕРЕНОСА ОТ РЯДА ДИСКРЕТНЫХ ИСТОЧНИКОВ В ГОРИЗОНТАЛЬНОМ КАНАЛЕ ПРЯМОУГОЛЬНОГО СЕЧЕНИЯ

Аннотация—Проведены эксперименты и трехмерные численные расчеты с целью исследования смешанноконвективного теплопереноса от 12 квадратных источников тепла, расположенных линейно в четыре ряда и установленных заподлицо с нижней стенкой горизонтального прямоугольного канала. Экспериментальные данные получены для режимов теплопереноса при чисто естественной, смешанной, вынужденной ламинарной конвекции, а также для режима начала перехода к турбулентности. Зависимость среднего по рядам значения числа Нуссельта от числа Рейнольдса имеет минимум, на основании чего можно предположить, что благодаря индуцированному подъемной силой течению возможно интенсифицировать теплоотдачу и снизить мощность прокачки за счет уменьшения скорости течения. Для характеристики интенсивности вторичного течения, обусловленного подъемной силой, и определения условий, при которых оно существенно, вводятся соответствующие масштабные параметры.